physica status solidi rrl
www.pss-rapid.com

Light-Assisted and Gate-Tunable Oxygen Gas Sensor Based on Rhenium Disulfide Field-Effect Transistors

Amir Zulkefli, Bablu Mukherjee, Ryoma Hayakawa, Takuya Iwasaki, Shu Nakaharai, and Yutaka Wakayama**

Gas sensors based on transition metal dichalcogenides (TMDCs) have attracted much attention from a new perspective involving light-assisted or gate-voltage operation. However, their combined roles as regards the gas sensing performance and mechanism are not yet understood due to the lack of controlled studies. This study systematically investigates the oxygen sensor performance and mechanism of few-layer-thick rhenium disulfide (ReS_2) field-effect transistors (FETs) under light illumination and gate biasing. As a result, a combination of light illumination and positive gate voltage enhances the device response over 100% at a 1% oxygen concentration; that is, the approach achieves a practical sensitivity of 0.01% ppm^{-1}, which outperforms most of the reports available in the literature. Furthermore, the fabricated devices exhibit long-term stability and stable operation even under humid conditions, indicating the ability of the sensor device to operate in a real-time application. These results contribute to the development of versatile tunable oxygen sensors based on TMDC FETs.

Oxygen sensors are essential for a wide range of applications related to, for example, medicine, automobiles, food, and the environment.[1–6] Over the past century, sensors have verified oxygen concentrations using chemical, optical, or electrical approaches.[7,8] Of these approaches, the field-effect transistor (FET) has been widely used in gas sensor applications.[9–11] This is because of its easy incorporation into integrated circuits and well-developed fabrication process. Moreover, current modulation by gate biasing and room-temperature operation provide the advantages of a long device lifetime and low power consumption.[12]

Currently, 2D materials are being intensively studied for use in gas sensor devices because of their chemical, physical, optical, and electronic features.[13–16] In other words, 2D materials are promising platforms for gas sensing devices because of their naturally high surface-area-to-volume ratio, which results in high sensitivity. In particular, transition metal dichalcogenides (TMDCs) have a finite bandgap in the 0.2–3.0 eV range depending on the constituent materials and their numbers of layers,[17–19] and they could be used for an FET-based gas sensor.

Although the enhancement of the gas sensitivity of TMDC-based FETs by light illumination and gate biasing[20–25] has been reported, the mechanism and roles of their combined effects are not yet understood. In this regard, among the TMDCs, rhenium disulfide (ReS_2) is a promising candidate for a light-assisted and gate-tunable oxygen sensor. This is because ReS_2 offers direct bandgap matching with the visible light range regardless of thickness unlike other TMDCs.[26–28] Therefore, ReS_2 is an ideal material that offers an optimal trade-off relation between the surface-area-to-volume ratio (thin layer required) and the charge carrier density with the optical absorption (thick layer required) toward realizing a high-performance gas sensor based on a light-assisted and gate-bias operation.

In this study, we investigated ReS_2 FET-based oxygen sensor devices. The sensing performance, including response, sensitivity, stability, and durability, was studied in a systematic manner. We focused particularly on the light illumination and gate voltage dependence to clarify their roles in the sensing mechanism. As a result, a practical sensitivity of 0.01% ppm^{-1} was achieved for oxygen gas by combining light illumination and a positive gate voltage, which outperform over previous reports.[29,30] This research also contributes to an in-depth understanding of the roles of light illumination and gate biasing, leading to the development of a high-performance gas sensor based on TMDC FETs.

Figure 1a shows a homemade chamber setup (dimensions: $9.0 \times 6.0 \times 2.5\ cm^3$) that we used for the ReS_2-FET-based oxygen sensor measurements (see the detailed preparation, fabrication, and sensing measurements of the sensor in the Experimental Section). Figure 1b shows a Raman spectrum of the ReS_2 nanosheet, which displays 18 first-order modes within 100−450 cm^{-1}. All the Raman peaks are of A_g symmetry.[31] This labeling Raman

A. Zulkefli, Dr. B. Mukherjee, Dr. R. Hayakawa, Dr. T. Iwasaki, Dr. S. Nakaharai, Prof. Y. Wakayama
International Center for Materials Nanoarchitectonics (MANA)
National Institute for Materials Science (NIMS)
1-1 Namiki, Tsukuba 305-0044, Japan
E-mail: NAKAHARAI.Shu@nims.go.jp; WAKAYAMA.Yutaka@nims.go.jp

A. Zulkefli, Prof. Y. Wakayama
Department of Chemistry and Biochemistry
Faculty of Engineering
Kyushu University
1-1 Namiki, Tsukuba 305-0044, Japan

Dr. T. Iwasaki
International Center for Young Scientists (ICYS)
National Institute for Materials Science (NIMS)
1-1 Namiki, Tsukuba 305-0044, Japan

The ORCID identification number(s) for the author(s) of this article can be found under https://doi.org/10.1002/pssr.202000330.

DOI: 10.1002/pssr.202000330

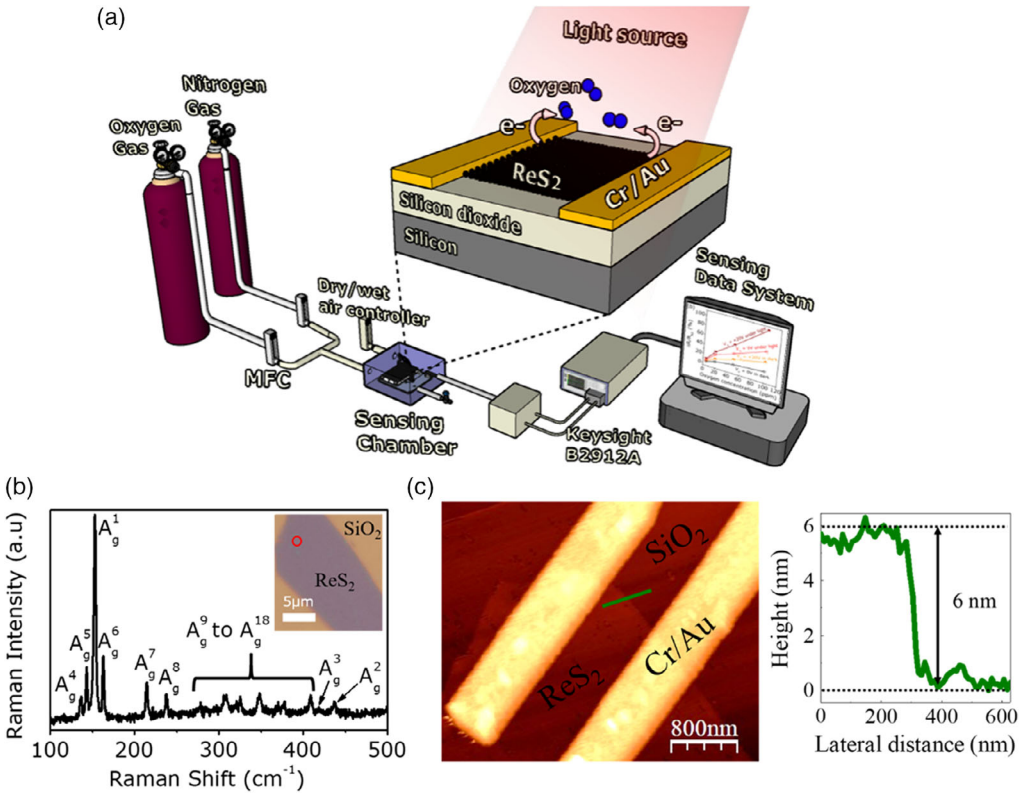

Figure 1. a) Schematic diagram of the homemade gas sensing measurement setup and the ReS_2 FET-based oxygen sensor. b) Raman spectrum of the ReS_2 nanosheet obtained at the location indicated by the red circle seen in the inset optical image. c) AFM image and height profile of the eight-layer ReS_2 nanosheet.

peaks scheme was adopted from the previous report.[32] The in-plane, out-of-plane, and quasi-out-of-plane modes near 150, 437, and 418 cm^{-1} are labeled as A_g^1, A_g^2, and A_g^3, respectively. This result confirmed the high crystallinity and chemical purity of the ReS_2 nanosheet.[33] Figure 1c shows an atomic force microscopy (AFM) image and the height profile (green line in the AFM image) of the ReS_2 nanosheet. The height profile confirmed that the ReS_2 thickness was ≈6 nm, corresponding to eight-layer-thick ReS_2. The eight-layer ReS_2 nanosheet was used for all the oxygen sensing measurements in this study, because this thickness was found to be optimal (see Figure S1, Supporting Information, for the thickness-dependent properties).

Initially, the transfer curve was measured in a dark condition without oxygen exposure as a reference, as shown in **Figure 2**a. A typical n-type operation was observed; i.e., electrons were majority carriers in the ReS_2 FET. Then, the influence of light illumination on oxygen sensing was examined. Figure 2b,c shows the output characteristics of the ReS_2 FET in dark conditions and under light illumination, respectively, while no gate voltage was applied. As shown in Figure 2b, the drain current gradually decreased, as the oxygen concentration increased from 0 to 10 000 ppm. These results were caused by the nature of the oxygen molecule as an electron acceptor.[34] That is, electrons were transferred from the ReS_2 channel surface to the physically adsorbed oxygen molecules to increase the device resistance.

This tendency was enhanced by light illumination, as shown in Figure 2c; the variations in the drain current were larger than those obtained under dark conditions. For a clear comparison, the response under both dark conditions and light illumination are plotted as a function of oxygen concentration in Figure 2d, where the oxygen response was determined as the resistance ratio $\left(\frac{\Delta R}{R_{N_2}}\right)$ based on the following equation

$$\frac{\Delta R}{R_{N_2}} = \left[\frac{R_{O_2} - R_{N_2}}{R_{N_2}} \times 100\right]\% \quad (1)$$

where R_{N_2} and R_{O_2} are the channel resistances in nitrogen gas (oxygen concentration = 0) and oxygen gas, respectively. The response under dark conditions (black line) showed a slightly monotonical increase from 4% to 19% with increasing oxygen concentration. Meanwhile, light illumination yielded a response of 60% at an oxygen concentration of 10 000 ppm, which is three times higher than that measured under dark conditions. This improvement was achieved by the photogenerated carriers.[35] That is, light illumination increased the electron population in the ReS_2 FET, and these electrons were available to interact with oxygen gas molecules. This result clearly demonstrates the advantage of light-assisted gas sensing. For these experiments, the light intensity was fixed at 8.4 mW cm^{-2}, because the maximum response was observed at this intensity (see Figure S2, Supporting Information, for more details).

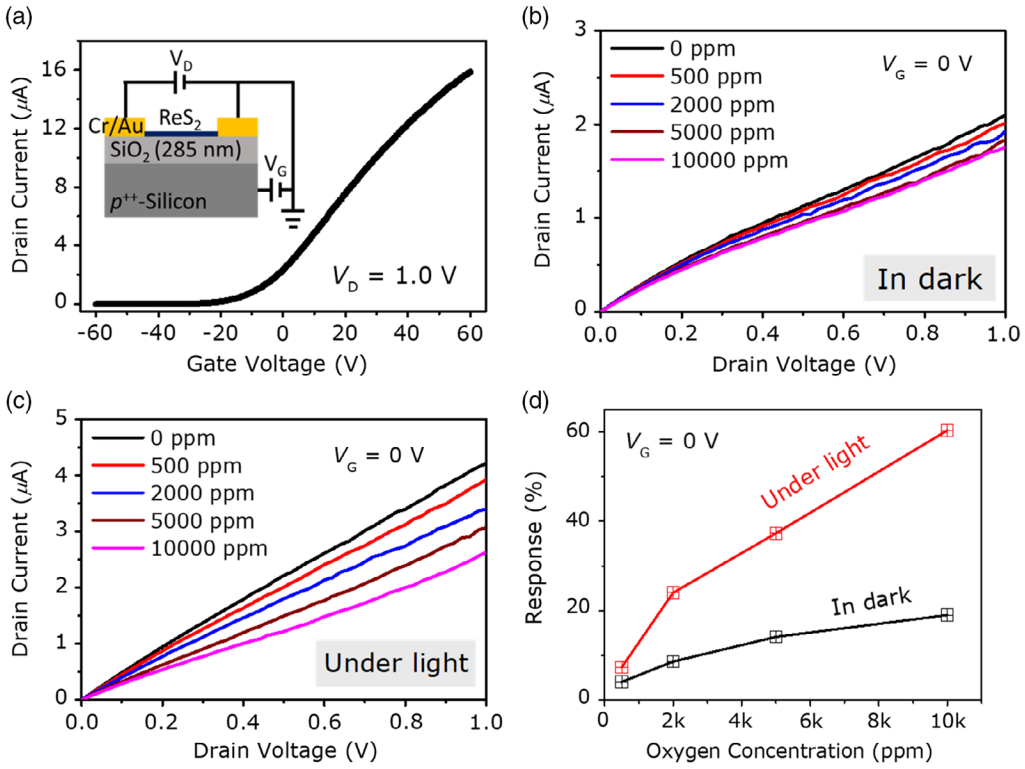

Figure 2. a) Transfer curve of the eight-layer ReS_2 FET, and its output characteristics b) in the dark and c) with light illumination. The O_2 gas concentration ranged from 0 to 10 000 ppm. No gate voltage was applied. d) Response as a function of O_2 gas concentration in the dark (black line) and with illumination (red line).

To examine the effect of the gate voltage on the oxygen sensing performance, the output characteristics were measured under dark conditions with negative ($V_G = -20$ V) and positive ($V_G = +20$ V) gate voltages, as shown in **Figure 3**a,b, respectively. As can be seen, the variations in the drain current with a negative gate voltage were marginal. Meanwhile, a clear modulation was observed in the drain current with a positive gate voltage. This tendency is further confirmed by the response-oxygen concentration curves shown in Figure 3c. Here, the curve without a gate voltage ($V_G = 0$, black line) is duplicated from Figure 2c for comparison. The response was increased by 38% by a positive gate voltage, whereas a negative gate voltage reduced it to 13% at a 10 000 ppm oxygen concentration. The results can also be explained in terms of the electron population at the ReS_2/SiO_2 interface. The negative gate voltage depleted the electrons at the ReS_2/SiO_2 interface. As a result, oxygen gas molecules, which are electron acceptors, receive fewer electrons from the ReS_2 FET. In the meantime, the electrons accumulated at the ReS_2/SiO_2 interface under a positive gate voltage to promote electron transfer with oxygen gas molecules, which contributed to the increment in oxygen gas response.

Next, we examined the combined effect of a positive gate voltage and light illumination on sensing performance. **Figure 4**a shows the output characteristics of the ReS_2 FET measured with

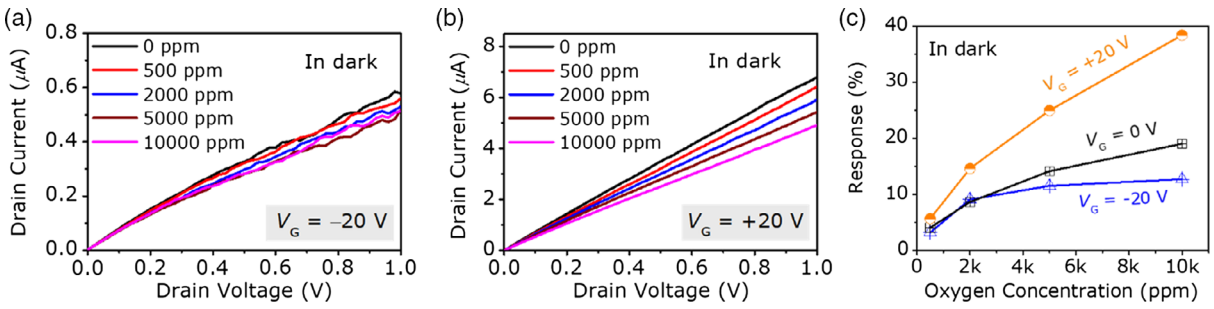

Figure 3. Output characteristics of the eight-layer ReS_2 FET under a) $V_G = -20$ V and b) $V_G = +20$ V, and O_2 gas exposure at the concentrations of 0–10 000 ppm measured in dark conditions. c) Response as a function of O_2 gas concentration curves of the sensor with and without applying a gate voltage in dark conditions.

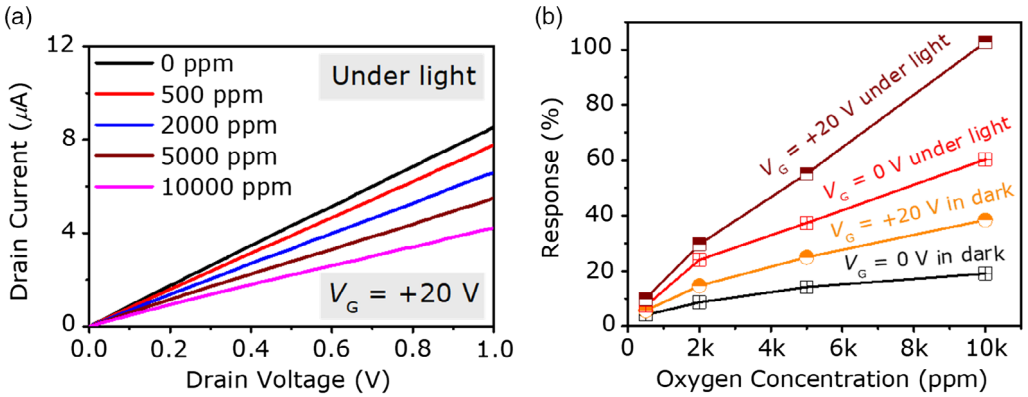

Figure 4. a) Output characteristic of the eight-layer ReS_2 FET where $V_G = +20$ V and in an O_2 gas atmosphere at various concentrations ranging from 0 to 10 000 ppm measured under light illumination. b) Response as a function of O_2 gas concentration when operated under various conditions: with/without gate voltage and with/without light illumination.

a combination of light illumination and a positive gate voltage ($V_G = +20$ V). We observed a distinct decrease in the drain currents with increasing oxygen concentration. Figure 4b summarizes response as a function of oxygen concentration. The ReS_2 FET operated under light illumination and a positive gate voltage exhibited improved oxygen gas response, which exceeded 100% at an oxygen concentration of 10 000 ppm. Namely, we achieved a sensitivity of 0.01% ppm^{-1}. This is higher than the value obtained in the dark with (0.003% ppm^{-1}) and without (0.002% ppm^{-1}) a gate voltage, and solely with light illumination (0.005% ppm^{-1}) (see Figure S3, Supporting Information, for more details).

As mentioned earlier, the gas response is strongly related to the electron population in the ReS_2 FET. These phenomena can be further understood from the band diagrams shown in **Figure 5**. These band diagrams illustrate the interaction of the electrons in the conduction band of ReS_2 with oxygen gas on the ReS_2 surface. Under dark conditions without gate biasing (Figure 5a), the response is predominantly influenced by the doping effect of the gas molecules.[36] Meanwhile, the positive gate biasing leads to electron accumulation in ReS_2, which decreases R_{N_2} (Figure 5b). Then, the ReS_2 surface attracts the oxygen molecules, resulting in an increase in ΔR. Thus, the response $\left(\frac{\Delta R}{R_{N_2}}\right)$ is enhanced. On the other hand, the light illumination also generates electrons by photoexcitation, leading to the enhancement of $\frac{\Delta R}{R_{N_2}}$ (Figure 5c). The response is further improved by the combination of positive gate biasing and light illumination, which cause both the capacitively induced and photoinduced electrons to accumulate (Figure 5d). Consequently, a huge $\frac{\Delta R}{R_{N_2}}$ enhancement is accomplished. The oxygen sensing performance in this study appears to be particularly noteworthy among reported sensors, which are summarized in Table S1, Supporting Information.

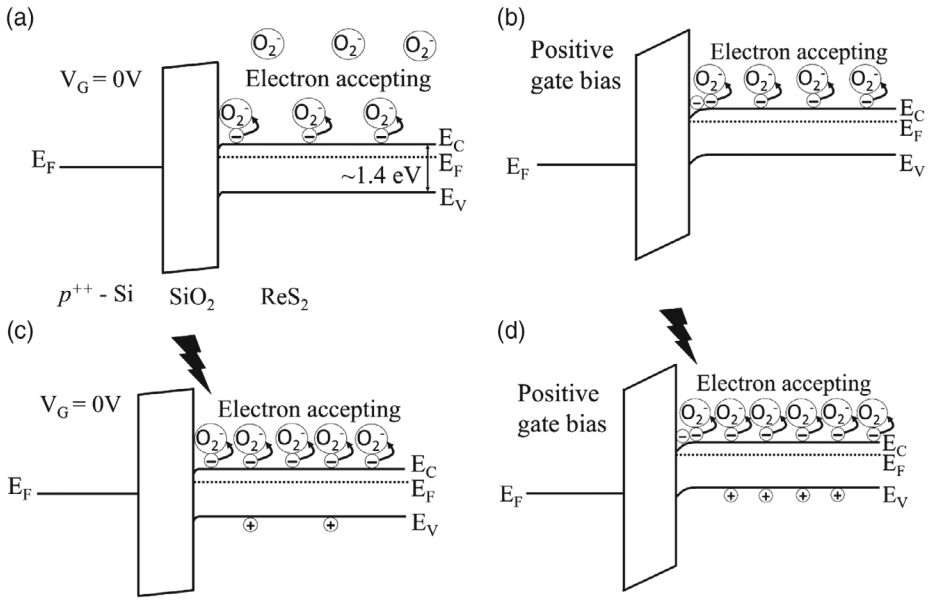

Figure 5. Band diagrams of the ReS_2 FET, illustrating the interaction of electrons in the ReS_2 with oxygen gas a) under dark conditions without a gate bias, b) under dark conditions with a positive gate bias, c) under light illumination without a gate bias, and d) under light illumination with a positive gate bias.

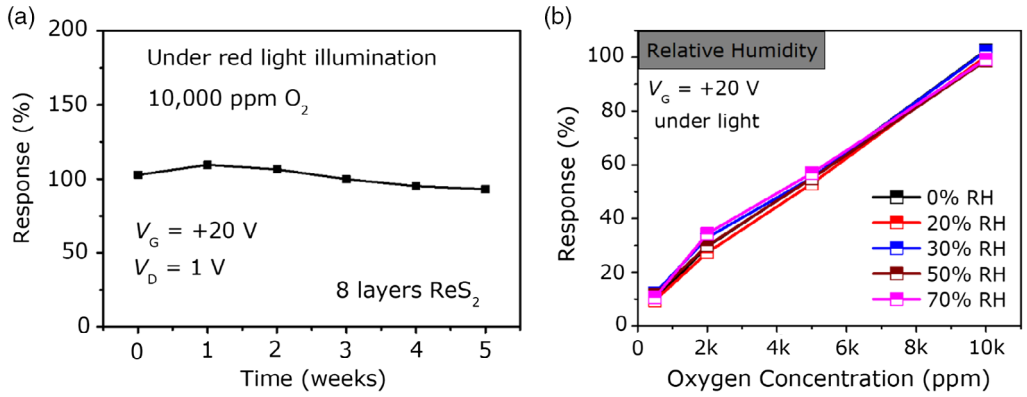

Figure 6. a) Long-term stability test at 10 000 ppm O_2 gas concentration. b) Influence of RH on device response. The RH was varied from 0% to 70% by controlling the mixture ratio of dry and wet air.

The stability and durability of the ReS_2 FET-based oxygen sensor properties are also vital for practical applications. To examine these factors, measurements were repeated in light illumination and positive gate voltage operations. The device was exposed to oxygen gas every week for 35 days in dry or humid conditions. As shown in **Figure 6**a,b, the response at an oxygen concentration of 10 000 ppm was retained after 35 days of measurement, and it was largely unchanged even when measured in humid conditions. That is, our sensor showed long-term stability and stable operation even under humid conditions. We suggest that this high stability is brought about by the advantages of gate biasing and light illumination in suppressing the electron transfer from the water molecules to the ReS_2 surface (see Figure S4, Supporting Information, for more details). The results imply that our sensor could be used in real-time applications.

In conclusion, we have developed high-performance ReS_2 FET-based oxygen sensors by combining light illumination and a gate biasing operation. The underlying mechanism was explained by the electron transfer from ReS_2 into oxygen molecules to stimulate changes in the transistor properties. Light illumination and gate biasing improved the oxygen sensing properties by increasing the photogenerated carrier and doping level of the ReS_2 FET. In consequence, a practical sensitivity of 0.01% ppm^{-1} was achieved, which outperform results from the previous reports. Furthermore, long-term stability and stable operation even under humid conditions enabled the sensor device to be used in real-time applications. These results imply that a light-assisted and gate-bias-tunable oxygen sensor based on a ReS_2 FET has the potential for allowing further sensor development toward versatile tunable oxygen sensors. Future studies are yet to be considered for further understanding on gas sensing properties of ReS_2 FET. This including the angle-dependent study of ReS_2 anisotropic crystal lattice structure on gas sensing performance.

Experimental Section

Preparation and Characterization of ReS_2 Nanosheets: ReS_2 nanosheets were prepared by a gold (Au)-mediated exfoliation method,[37] which was effective for preparing large-scale ReS_2 nanosheets with a uniform thickness. With this method, a bulk ReS_2 crystal (HQ graphene supplier) was mechanically exfoliated on a thermal tape (Nitto Denko, model NO319Y-4LSC). A 100 nm-thick Au film was then evaporated directly onto an as-exfoliated ReS_2/thermal tape. Another thermal tape was used to exfoliate Au/ReS_2 layers from the initial ReS_2/Au coated thermal tape, and then, the exfoliated Au/ReS_2 layers were pasted onto SiO_2/Si substrates. Next, the thermal tape was detached at a temperature of 100 °C. Finally, the substrate was immersed in Au etchant (AURUM-302, Kanto Chemical: etching rate is 100 nm min^{-1}) for 4 min and then rinsed in deionized water for 5 min to fully remove the residual Au layer from the ReS_2 surface. To exclude the effect of any residues that might come from this method on the sensing performance, an elemental analysis of Au-mediated exfoliated bulk ReS_2 was carried out by scanning electron microscopy-energy dispersive X-ray (SEM-EDX) (see Figure S5, Supporting Information, for more details). The crystallinity and film thickness of thus prepared ReS_2 nanosheets were characterized by Raman microscopy (Nanophoton, model: Ramanplus) and AFM. To avoid any possible effect of heating on the ReS_2 nanosheets, the Raman laser power on the sample was fixed at 1 mW. The fabrication process and an optical image are shown in Figure S6, Supporting Information.

Fabrication of ReS_2 FET-Based Oxygen Sensor: To fabricate the FET-based sensor, a SiO_2/Si substrate with ReS_2 nanosheets was coated with a polymethyl methacrylate layer and patterned using electron-beam lithography (Elionics, ELS-7000), followed by Cr/Au (3/80 nm) metal deposition using e-beam evaporation and a liftoff process. The ReS_2 channel length and width were 0.65 and 2 μm, respectively. Here, the highly doped Si substrate and the 285 nm-thick SiO_2 layer worked as a gate electrode and a gate dielectric layer, respectively. The sample device was then cut to form a 2.5 × 2.5 mm^2 chip using a manual scribing machine and was mounted on an eight-pin standard chip carrier using silver paste. A manual wedge-wedge bonder was utilized to realize a wire-bond connection between the chip carrier and the sensor device.

Sensing Measurement of ReS_2 FET-Based Oxygen Sensor: The homemade gas measurement setup was equipped with a mixing connector linked to mass flow controllers that made it possible to adjust the oxygen concentration by changing the O_2/N_2 gas mixing ratio. A constant flow rate of 100 mL min^{-1} was used for dry air and oxygen gas. The gas chamber was flushed with nitrogen for a few hours to recover the device to the initial state after each measurement. The setup was also equipped with a relative humidity (RH) controller. The RH levels were monitored with a commercial humidity sensor. All the current–voltage (I–V) measurements were carried out at room temperature using a source-measurement unit (Keysight B2912A), which was connected to a data acquisition system using EasyEXPERT software. A Xenon lamp (Asahi spectra Co. Ltd., MAX 303) was used for light irradiation. The sensor was illuminated with red light at a wavelength of 650 nm (Figure S7, Supporting Information) through the acrylic resin window of the gas sensor chamber. The light intensity was monitored with a power meter (Ophir Optics, PD300).

Supporting Information

Supporting Information is available from the Wiley Online Library or from the author.

Acknowledgements

This research was supported by the World Premier International Center (WPI) for Materials Nanoarchitectonics (MANA) of the National Institute for Materials Science (NIMS), Tsukuba, Japan. A part of this study was supported by a Grant-in-Aid for Scientific Research (JSPS KAKENHI Grant No./Project/Area No.17F17360), and the NIMS Nanofabrication Platform and the NIMS Molecule & Material Synthesis Platform in the Nanotechnology Platform Project sponsored by the Ministry of Education, Culture, Sports, Science, and Technology (MEXT), Japan.

Conflict of Interest

The authors declare no conflict of interest.

Keywords

field-effect transistors, gate tunability, light-assisted operation, oxygen sensors, rhenium disulfide

Received: July 4, 2020
Revised: August 7, 2020
Published online: September 16, 2020

[1] Y. Liu, J. Parisi, X. Sun, Y. Lei, *J. Mater. Chem. A* **2014**, *2*, 9919.
[2] A. W. Hempel, D. B. Papkovsky, J. P. Kerry, *Foods* **2013**, *2*, 507.
[3] C. Chou, Y. Wu, C. Lin, *RSC Adv.* **2014**, *4*, 52903.
[4] C. A. Kelly, E. Santovito, M. Cruz-Romero, J. P. Kerry, D. P. Papkovsky, *Sens. Actuators, B* **2020**, *304*, 127338.
[5] J. D. Spengler, K. Sexton, *Science* **1993**, *221(4605)*, 9.
[6] M. Bartic, *Phys. Status Solidi A* **2016**, *213*, 457.
[7] M. Stoeckel, M. Gobbi, S. Bonacchi, F. Liscio, L. Ferlauto, E. Orgiu, P. Samorì, *Adv. Mater.* **2017**, *29*, 1702469.
[8] X. Wang, O. S. Wolfbeis, *Chem. Soc. Rev.* **2014**, *43*, 3666.
[9] X. Liu, T. Ma, N. Pinna, J. Zhang, *Adv. Funct. Mater.* **2017**, *27*, 1702168.
[10] S. Mao, J. Chang, H. Pu, G. Lu, Q. He, H. Zhang, J. Chen, *Chem. Soc. Rev.* **2017**, *46*, 6872.
[11] S. Yuvaraja, S. G. Surya, M. T. Vijjapu, V. Chernikova, O. Shekhah, M. Eddaoudi, K. N. Salama, *Phys. Status Solidi RRL* **2020**, 2000086.
[12] X. Zhao, B. Cai, Q. Tang, Y. Tong, Y. Liu, *Sensors* **2014**, *14*, 13999.
[13] D. Akinwande, C. Huyghebaert, C. H. Wang, M. I. Serna, S. Goossens, L. J. Li, H. S. P. Wong, F. H. L. Koppens, *Nature* **2019**, *573(7775)*, 507.
[14] E. Lee, Y. S. Yoon, D.-J. Kim, *ACS Sens.* **2018**, *3*, 2045.
[15] M. J. Kang, J. Y. Kim, J. Seo, S. Lee, C. Park, S. M. Song, S. S. Kim, M. G. Hahm, *Phys. Status Solidi RRL* **2019**, *13*, 1900340.
[16] D. Yu, J. Li, T. Wang, X. She, Y. Sun, J. Li, L. Zhang, X. F. Yu, D. Yang, *Phys. Status Solidi RRL* **2020**, *14*, 1900697.
[17] D. Ovchinnikov, A. Allain, Y. S. Huang, D. Dumcenco, A. Kis, *ACS Nano* **2014**, *8*, 8174.
[18] S. Manzeli, D. Ovchinnikov, D. Pasquier, O. V. Yazyev, A. Kis, *Nat. Rev. Mater.* **2017**, *2*, 17033.
[19] M. Chhowalla, Z. Liu, H. Zhang, *Chem. Soc. Rev.* **2015**, *44*, 2584.
[20] W. J. Yan, D. Y. Chen, H. R. Fuh, Y. L. Li, D. Zhang, H. Liu, G. Wu, L. Zhang, X. Ren, J. Cho, M. Choi, B. S. Chun, C. Coileáin, H. J. Xu, Z. Wang, Z. Jiang, C. R. Chang, H. C. Wu, *RSC Adv.* **2019**, *9*, 626.
[21] M. Kumar, A. V. Agrawal, R. Kumar, S. Venkatesan, A. Zakhidov, G. Yang, J. Bao, M. Kumar, *ACS Sens.* **2018**, *3*, 998.
[22] S. Yang, J. Kang, Q. Yue, J. M. D. Coey, C. Jiang, *Adv. Mater. Interfaces* **2016**, *3*, 1500707.
[23] Z. Feng, Y. Xie, J. Chen, Y. Yu, S. Zheng, R. Zhang, Q. Li, X. Chen, C. Sun, H. Zhang, W. Pang, J. Liu, D. Zhang, *2D Mater.* **2017**, *4*, 025018.
[24] X. Yan, Y. Wu, R. Li, C. Shi, R. Moro, Y. Ma, L. Ma, *ACS Omega* **2019**, *4*, 14179.
[25] T. Pham, G. Li, E. Bekyarova, M. E. Itkis, A. Mulchandani, *ACS Nano* **2019**, *13*, 3196.
[26] S. Tongay, H. Sahin, C. Ko, A. Luce, W. Fan, K. Liu, J. Zhou, Y. S. Huang, C. H. Ho, J. Yan, D. F. Ogletree, S. Aloni, J. Ji, S. Li, J. Li, F. M. Peeters, J. Wu, *Nat. Commun.* **2014**, *5*, 3252.
[27] Y. Xiong, H. W. Chen, D. W. Zhang, P. Zhou, *Phys. Status Solidi RRL* **2019**, *13*, 1800658.
[28] P. Nagler, G. Plechinger, C. Schüller, T. Korn, *Phys. Status Solidi RRL* **2016**, *10*, 185.
[29] Y. Tong, Z. Lin, J. T. L. Thong, D. S. H. Chan, C. Zhu, *Appl. Phys. Lett.* **2015**, *107*, 123105.
[30] N. Sakhuja, R. K. Jha, R. Chaurasiya, A. Dixit, N. Bhat, *ACS Appl. Nano Mater.* **2020**, *3*, 3382.
[31] N. R. Pradhan, A. McCreary, D. Rhodes, Z. Lu, S. Feng, E. Manousakis, D. Smirnov, R. Namburu, M. Dubey, A. R. H. Walker, H. Terrones, M. Terrones, V. Dobrosavljevic, L. Balicas, *Nano Lett.* **2015**, *15*, 8377.
[32] A. McCreary, J. R. Simpson, Y. Wang, D. Rhones, K. Fujisawa, L. Balicas, M. Dubey, V. H. Crespi, M. Terrones, A. R. H. Walker, *Nano Lett.* **2017**, *17*, 5897.
[33] B. Mukherjee, A. Zulkefli, R. Hayakawa, Y. Wakayama, S. Nakaharai, *ACS Photonics* **2019**, *6*, 2277.
[34] J. Zhang, C. Zhao, P. A. Hu, Y. Q. Fu, Z. Wang, W. Cao, B. Yang, F. Placido, *RSC Adv.* **2013**, *3*, 22185.
[35] N. Huo, S. Yang, Z. Wei, S.-S. Li, J.-B. Xia, J. Li, *Sci. Rep.* **2014**, *4*, 5209.
[36] Y. Cai, Q. Ke, G. Zhang, Y. W. Zhang, *J. Phys. Chem. C* **2015**, *119*, 3102.
[37] S. B. Desai, S. R. Madhvapathy, M. Amani, D. Kiriya, M. Hettick, M. Tosun, Y. Zhou, M. Dubey, J. W. Ager, D. Chrzan, A. Javey, *Adv. Mater.* **2016**, *28*, 4053.